Inorganic Chemistry

Article

pubs.acs.org/IC

Biotransformations of Antidiabetic Vanadium Prodrugs in Mammalian Cells and Cell Culture Media: A XANES Spectroscopic Study

Aviva Levina, Andrew I. McLeod, Anna Pulte, Jade B. Aitken, and Peter A. Lay*

School of Chemistry, The University of Sydney, Sydney, New South Wales 2006, Australia

Supporting Information

ABSTRACT: The antidiabetic activities of vanadium(V) and -(IV) prodrugs are determined by their ability to release active species upon interactions with components of biological media. The first X-ray absorption spectroscopic study of the reactivity of typical vanadium (V) antidiabetics, vanadate ($[V^VO_4]^{3-}$, **A**) and a vanadium(IV) bis(maltolato) complex (**B**), with mammalian cell cultures has been performed using HepG2 (human hepatoma), A549 (human lung carcinoma), and 3T3-L1 (mouse adipocytes and preadipocytes) cell lines, as well as the corresponding cell culture media. X-ray absorption near-edge structure data were analyzed using empirical correlations with a library of model vanadium(V), -(IV), and -(III) complexes. Both **A** and **B** ([V] = 1.0 mM) gradually converged into similar mixtures of predominantly five- and six-coordinate V^V species (~75% total V) in a cell culture medium within 24 h at 310 K. Speciation of V in intact HepG2 cells also changed with the incubation time (from ~20% to ~70% V^{IV} of total V), but it was largely independent of the prodrug used (**A** or **B**) or of the predominant V oxidation state in the medium. Subcellular fractionation of A549 cells suggested that V^V reduction to V^{IV} occurred predominantly in the cytoplasm, while accumulation of V^V in the nucleus was likely to have been facilitated by noncovalent bonding to histone proteins. The nuclear V^V is likely to modulate the transcription process and to be ultimately related to cell death at high concentrations of V, which may be important in anticancer activities. Mature 3T3-L1 adipocytes (unlike for preadipocytes) showed a higher propensity to form V^{IV} species, despite the prevalence of V^V in the medium. The distinct V biochemistry in these cells is consistent with their crucial role in insulin-dependent glucose and fat metabolism and may also point to an endogenous role of V in adipocytes.

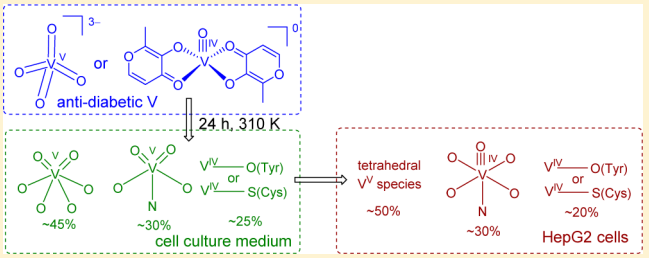

INTRODUCTION

Although the antidiabetic activity of vanadium(V) has been known for over a century,[1] its systematic exploration started from the discovery in the early 1980s[1] of the role of vanadate ($[V^VO_4]^{3-}$, **A** in Chart 1) as a powerful inhibitor of protein tyrosine phosphatases (PTPs),[2] which act as negative regulators (deactivators) of the insulin signaling cascade.[3] Most of the recent studies have focused on the development of vanadium-(IV) or -(V) complexes with organic ligands [such as a vanadium(IV) bis(maltolato) complex, **B** in Chart 1] as delivery agents that improve gastrointestinal absorption and reduce the toxicity of vanadate.[1,4−7] The role of such complexes as prodrugs that release the active component upon interactions with biological media has been established based on the following evidence: (i) animal studies using ^{48}V- and ^{14}C-labeled vanadium(IV) complexes showed that these prodrugs decomposed shortly after ingestion, particularly when administered together with food;[1,8,9] (ii) similar antidiabetic activities were found in animal experiments[5] and cell assays[10] using a wide variety of vanadium(V), -(IV), and -(III) complexes with organic ligands, which indicated that these compounds converged to similar products upon reactions with biological media;[5,11] (iii) stable nonoxidovanadium(IV) complexes that did not dissociate in aqueous media also did not show any antidiabetic activity in cell assays;[12] (iv) reaction of **B** with recombinant human PTP1B (a crucial phosphatase involved in insulin signaling) in an aerated aqueous solution at pH ~ 8 resulted in the formation of a PTP1B adduct with **A** (characterized by protein crystallography).[13]

Until recently, most of the speciation studies of biologically relevant vanadium(V) and -(IV) complexes have been performed with model systems (e.g., isolated proteins in aqueous buffers), using either electron paramagnetic resonance (EPR) or ^{51}V NMR spectroscopies, which are specific for V^{IV} and V^V ions, respectively.[14−17] In the past decade, X-ray absorption spectroscopy (XAS), including X-ray absorption near-edge structure (XANES) and extended X-ray absorption fine structure (EXAFS) spectroscopies, has become a leading tool for the speciation studies of metal ions in biological matrixes.[5,11,18−20] The advantages of XANES spectroscopy for vanadium(V) speciation studies are the following: (i) simultaneous determination and quantitation of biologically

Received: December 3, 2014
Published: April 23, 2015

DOI: 10.1021/ic5028948
Inorg. Chem. 2015, 54, 6707−6718

Chart 1. Structures of Vanadium(V) and -(IV) Complexes Used for Reactions with Cell Cultures (A and B), Additional Model Complexes Used in the Data Analysis (C−I),[21] and Typical Vanadium(IV) and -(V) Thiolato Complexes: $[V^{IV}O(dedtc)_2]$ [dedtc = Diethyldithiocarbamato(−)][34] and $(NEt_4)_2[V^V_2(O)_4(met)_2]_2$ [met = 2-Mercaptoethanolato(2−)][35a]

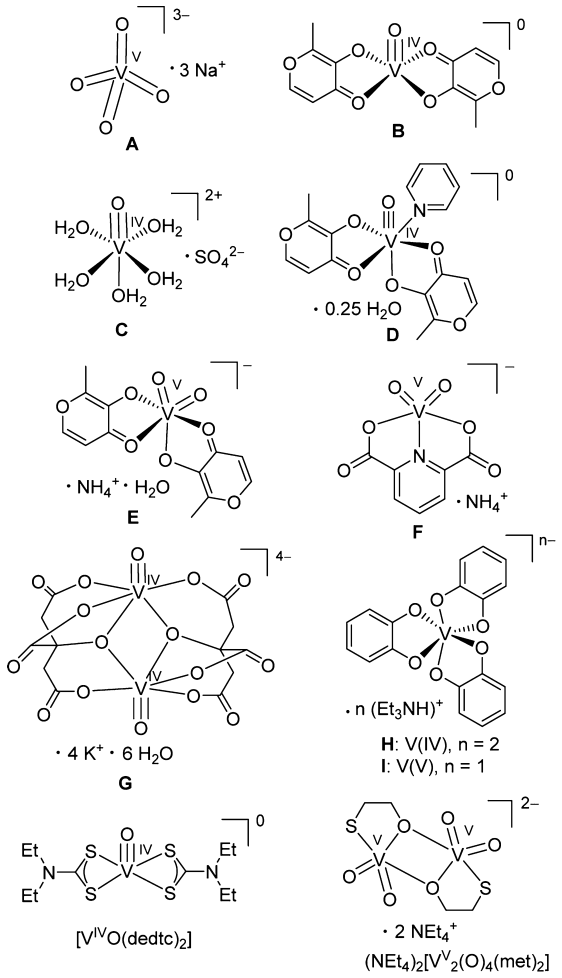

[a]Note that for monooxido complexes there is a triple bond consisting of one σ and two π bonds,[38] and the actual bond orders in vanadium(IV) and -(V) oxido complexes decrease as the number of oxido groups increases. While the vanadium oxido groups are shown as double bonds in the *cis*-dioxido species, the bond lengths are only slightly longer and the bond order should be considered as 2.5, whereas for **A**, they increase further and are double bonds.[38]

relevant V^V, V^{IV}, and V^{III} oxidation states; (ii) high sensitivity of XANES to the changes in the oxidation states, coordination numbers, and nature of donor atoms in vanadium complexes; (iii) the ability to use any matrixes, including intact cells and tissues; (iv) lower V detection limits compared to the traditional techniques, particularly when freeze-dried samples are used.[19,21−24] However, changes of V speciation induced by the X-ray beam (usually photoreduction) remain a serious problem that has to be addressed in such studies.[23,24]

Previously we developed an improved empirical method for determination of the V oxidation states and coordination numbers and the presence or absence of oxido ligands, using a library of biologically relevant vanadium(V), -(IV), and -(III) complexes.[21] This method was then used to examine the speciation of typical antidiabetic vanadium(V) and -(IV) complexes in artificial digestion systems[22] and in whole blood and its components.[23] This work focused on the reactivity of two archetypal V antidiabetics, **A** and **B** (Chart 1) in mammalian cell cultures, including cell culture media. Cell-based assays are widely used in the preclinical development of V antidiabetics,[10,25] but the associated biotransformations of vanadium complexes are poorly understood,[5,26] as is generally the case for metal-based pharmaceuticals.[19] The choice of cell lines for this study was as follows: (i) HepG2 human hepatoma cells[27] were used because of the crucial role of liver tissue in general drug metabolism,[28] as well as in glucose metabolism;[29] (ii) 3T3-L1 mouse adipocytes[30] were used because of the importance of adipose tissue in glucose metabolism and in the development of type 2 diabetes;[31] (iii) A549 human lung carcinoma cells[32] were used for comparison with the previous studies of our group on metal biotransformations in cultured cells.[18,19] V metabolism in cancer cell lines (HepG2 and A549) is also important because of the known anticancer properties of certain V prodrugs.[4]

EXPERIMENTAL SECTION

Model Complexes. The vanadium(V) and -(IV) complexes used for reactions with cultured mammalian cells (**A** and **B** in Chart 1) were either purchased from Aldrich (**A**, purity >99%) or synthesized by a literature procedure (**B**)[33] and characterized by elemental analyses and IR spectroscopy, as described previously.[21] A model vanadium(IV) thiolato complex, $[V^{IV}O(dedtc)_2]$ [Chart 1; dedtc = diethyldithiocarbamato(−)], was synthesized by a modified literature procedure[34] [see the Supporting Information (SI) for details], and its purity was confirmed by single-scattering analysis of EXAFS data (Figure S1 in the SI; application of other characterization techniques was difficult because of the air sensitivity of the complex). A model vanadium(V) thiolato complex, $(NEt_4)_2[V_2^V(O)_4(met)_2]$ [Chart 1; met = 2-mercaptoethanolato(2−)],[35] was synthesized and characterized as described previously.[21] Aqueous solutions of V^V met and V^V-GSH complexes (GSH = glutathione = γ-Glu-Cys-Gly) were generated according to the literature method[36] by reactions of Na_3VO_4 (10 mM) with thiol (12 mM) in an unbuffered solution (pH 7.7) for ∼1 min at 295 K and then freezing the reaction product at 77 K for XAS. The reaction products of **A** and **B** with HEPES-buffered saline [HBS, containing 20 mM HEPES, 140 mM NaCl, pH 7.40, where HEPES = 4-(2-hydroxyethyl)-1-piperazineethanesulfonic acid][37] were prepared by dissolution of solid **A** or **B** in HBS to $[V]_{final}$ = 1.0 mM; the resultant solutions were immediately frozen at ∼195 K and freeze-dried (217 K and 0.5 mbar for 16 h).[22] Dissolution of **B** was performed under a stream of argon in order to avoid V^{IV} oxidation to V^V.[33] The XANES spectra of the resultant solids (designated as **A*** and **B*** in the Results section) were used in data analysis, along with the previously reported[21] XANES spectra of other model complexes (**C**−**I** in Chart 1). Note that vanadium oxido bond orders in vanadium(IV) and -(V) complexes in Chart 1 (except for **A**) are greater than 2 (typically, 3 for monooxido and close to 2.5 for *cis*-dioxido complexes), which arise from a combination of one σ and two π bonds.[38]

Preparation of Biological Samples. A summary of conditions for sample preparation is given in Table 1. The HepG2 (human hepatoma),[27] 3T3-L1 (mouse preadipocyte),[30] and A549 (human lung adenocarcinoma)[32] cell lines were originally received from the American Type Culture Collection (ATCC) and cultured for 5−10 passages prior to the experiments. These cells were cultured in monolayers in Dulbecco's modified Eagle's medium (DMEM)[39] for 3T3-L1 cells or in Advanced DMEM[40] for HepG2 and A549 cells, supplemented with L-glutamine (2.0 mM), an antibiotic−antimycotic mixture (100 U mL^{-1} penicillin, 100 mg mL^{-1} streptomycin, and 0.25 mg mL^{-1} amphotericin B), and fetal calf serum [heat-inactivated; 2% (v/v) for HepG2 and A549 cells and 10% (v/v) for 3T3-L1 cells]. This medium is referred to below as the growth medium. Advanced

DOI: 10.1021/ic5028948
Inorg. Chem. 2015, 54, 6707−6718

Table 1. Description of the Biological Samples

designation[a]	preparation conditions[b]	V content[c,d,e]	beamline[g]
A1, **B1**	1.0 mM V, newborn calf serum (4 h at 310 K)	20 ± 5[d]	ANBF, SSRL
A2a, **B2a**	1.0 mM V, advanced DMEM, 2% serum (4 h at 310 K)	55 ± 5[d]	ANBF
A2b, **B2b**	1.0 mM V, advanced DMEM, 2% serum (8 h at 310 K)	54 ± 5[d]	ANBF
A2c, **B2c**	1.0 mM V, advanced DMEM, 2% serum (16 h at 310 K)	52 ± 6[d]	ANBF
A2d, **B2d**	1.0 mM V, advanced DMEM, 2% serum (24 h at 310 K)	52 ± 4[d]	ANBF
A3a, **B3a**	HepG2 cells, 1.0 mM V, complete medium, 4 h, 310 K	8.2 ± 1.2 (**A3a**)[e] 10.9 ± 0.8 (**B3a**)[e]	SSRL
A3b, **B3b**	HepG2 cells, 1.0 mM V, complete medium, 8 h, 310 K	4.8 ± 0.6 (**A3b**)[e] 8.2 ± 1.1 (**B3b**)[e]	SSRL
A3c, **B3c**	HepG2 cells, complete medium, 1.0 mM V, 16 h, 310 K	9.7 ± 1.2[e]	SSRL
A3d, **B3d**	HepG2 cells, complete medium, 1.0 mM V, 24 h, 310 K	7 ± 3[d] 12.3 ± 2.4[e]	SSRL
A4a	A549 cells, 1.0 mM **A** for 24 h (whole cells)	2.0 ± 0.4[e]	SSRL
A4b	A549 cells, 1.0 mM **A** for 24 h (nuclear fraction)	not measured[f]	SSRL
A4c	A549 cells, 1.0 mM **A** for 24 h (low-molecular-mass cytoplasmic fraction)	not measured[f]	SSRL
A5a	3T3-L1 cells (differentiated), 1.0 mM **A**[h] in a complete medium for 24 h	7.2 ± 1.1[e]	ANBF
A5b	3T3-L1 cells (undifferentiated), 1.0 mM **A** in a complete medium for 8 h	3.5 ± 0.5[e]	SSRL
A5c	3T3-L1 cells (undifferentiated), 0.10 mM **A** in a complete medium for 72 h	2.8 ± 0.4[e]	SSRL
A6a	1.0 mM **A**, DMEM, 10% serum (24 h at 310 K)	45 ± 5[d]	ANBF

[a]Designations of the vanadium complexes **A** and **B** correspond to those in Chart 1. [b]All of the samples were freeze-dried after the reactions (15 h at 220 K; see the Experimental Section for details). [c]Averages and standard deviations for three aliquots of the same sample; see the Experimental Section for details. [d]Values in nmol of V per mg of solid (measured by GFAAS; see the Experimental Section). [e]Values in nmol of V per mg of protein (measured by GFAAS and Bradford assays).[42] [f]Determination of the V content was difficult because of the small sample size. [g]Beamlines at which XANES data were collected: ANBF = Australian National Beamline Facility, Photon Factory, Tsukuba, Japan; SSRL = Stanford Synchrotron Research Lightsource, Stanford, CA. [h]Data for the cell samples treated with either 0.50 or 2.0 mM **A** were also collected (Figure S6a in the SI).

DMEM is supplemented with very low concentrations of vanadate (~2.5 nM),[40] but this did not cause an observable X-ray fluorescence signal in cell or media samples in the absence of added V compounds (data not shown). Cells were seeded in the growth medium at a density of ~5×10^5 cells per 75 cm^2 cell culture flask, grown at 310 K in a 5% CO_2-humidified incubator, and subcultured to 80–90% confluence (HepG2 and A549 cells) or to 60–70% confluence (3T3-L1 cells; the lower density was essential in order to prevent premature differentiation). Differentiation of 3T3-L1 cells into adipocytes (showing prominent fat droplets) was induced, in accordance with the literature method,[41] by growing the cells to 100% confluence (day 1), followed by treatment, on day 2, with the growth medium containing insulin (3.5×10^{-7} M), *iso*-butyl-1-methylxanthine (5.0×10^{-4} M), dexamethasone (2.5×10^{-7} M), and biotin (4.0×10^{-7} M).

This differentiation medium was replaced, on day 5, with a postdifferentiation medium (growth medium containing 3.5×10^{-7} M of insulin only), which was followed, on day 8, with a normal growth medium (see above), which was replaced every 2–3 days. The maximal yield of mature adipocytes (~95%) was reached on day 18, when the cells were treated with **A** (0.50, 1.0, or 2.0 mM) in the growth medium for 24 h at 310 K (samples **A5a** in Table 1). Alternatively, undifferentiated 3T3-L1 cells were treated with **A** in the growth medium (1.0 mM for 8 h or 0.10 mM for 72 h at 310 K) on day 1 (samples **A5b** and **A5c** in Table 1). Nondifferentiating HepG2 cells were treated with **A** or **B** (1.0 mM in the growth medium, 4–24 h at 310 K) on reaching ~80% confluence in 75 cm^2 flasks (samples **A3a**–**A3d** and **B3a**–**B 3d** in Table 1). After treatment for a specified time (Table 1), the V-containing medium was removed, the cells were washed three times with phosphate-buffered saline, trypsinized, pelleted by gentle centrifugation (1000*g* for 5 min at 298 K), and freeze-dried for XANES spectroscopy. Aliquots (1.0 mL) of V-containing growth media were collected after the treatment of HepG2 cells with V and freeze-dried for XANES spectroscopy (samples **A2a**–**A2d** and **B2a**–**B2d** in Table 1). A sample of the cell culture medium was also collected for the treatment of differentiated 3T3-L1 adipocytes with 1.0 mM **A** (**A6a** in Table 1). Treatments of A549 cells with **A** (1.0 mM in the growth medium, 24 h at 310 K) and isolation of whole cells and subcellular fractions (nuclear and high- and low-molecular-mass cytoplasmic) were performed as described previously for chromium(VI) treatments (samples **A4a**–**A4c** in Table 1).[18] The V levels in the high-molecular-mass cytoplasmic fraction were below the detection limit of XANES spectroscopy under the conditions used in these studies. A sterile stock solution of **A** (100 mM) in water was used for the cell treatments, while solid **B** was dissolved in the cell culture medium (to [V] = 1.0 mM) under sterile conditions immediately prior to the cell treatments. Although no significant cell detachment occurred in any of the treatments, signs of V toxicity (rounding of the cells) were visible for the treatments that lasted longer than 8 h. Treatments of newborn calf serum (heat-inactivated and aseptically filtered; purchased from Invitrogen) with either **A** or **B** (1.0 mM V for 4 h at 310 K; samples **A1** and **B1** in Table 1) were performed as described elsewhere.[23]

The V content in freeze-dried biological samples (Table 1) was determined by graphite furnace atomic absorption spectrometry (GFAAS) using a Varian SpecAA-20 spectrometer. Three aliquots of each sample (~1.0 mg) were weighed with ±0.01 mg precision, then digested with ultrapure HNO_3 [0.20 mL, 69% (w/v) in H_2O, Merck] by sonication (1 h at 50 W and 298 K), and brought to 1.0 mL volume with an ultrapure HCl solution [0.10 M, prepared from 37% (w/v) stock, Merck] for GFAAS analysis. Spectrometer calibrations were performed using a standard V^{IV} solution (1000 mg L^{-1}, Aldrich) diluted to 0.10–0.50 mg L^{-1} with an ultrapure HCl solution (0.10 M). Because determination of the V content in the cell samples by this method was difficult due to the small sample sizes (only **A3d** and **B3d** were used; see Table 1), the V uptake by cells was measured in relation to their protein content (Table 1). Each of the freeze-dried cell samples (after XANES spectroscopy) was divided into three aliquots (~0.05–0.2 mg each), and the aliquots were lysed in a 0.10 M NaOH solution (0.10 mL; prepared from 99.99% NaOH, Aldrich) by sonication (1 h at 50 W and 298 K). A part of the resulting lysate (0.050 mL) was mixed with HNO_3 (0.20 mL of 69%), followed by further sonication and determination of the V content by GFAAS, as described above, and the remaining lysate was used for protein determination by the Bradford method,[42] using bovine serum albumin (Sigma catalog no. A7030) as a standard.

XAS and Data Processing. V K-edge spectra of biological samples were recorded at the Australian National Beamline Facility (ANBF; beamline 20B at the Photon Factory, Tsukuba, Japan), or at beamline 9-3 at the Stanford Synchrotron Radiation Lightsource (SSRL), as indicated in Table 1. The beam energy was 2.5 GeV (ANBF) or 3.0 GeV (SSRL), and the maximal beam current was 400 mA (ANBF) or 200 mA (SSRL). Harmonic rejection was achieved at ANBF by detuning the channel-cut Si(111) monochromator by 50%. Beamline 9-3 at SSRL had a double-crystal Si(220) monochromator, an

DOI: 10.1021/ic5028948
Inorg. Chem. 2015, 54, 6707–6718

upstream collimating mirror, and a downstream sagittally focusing mirror; both mirrors were rhodium-coated and also provided harmonic rejection. Samples prepared according to Table 1 (as well as **A*** and **B***) were pressed into 0.5-mm-thick pellets that were supported within an aluminum spacer between two 63.5-μm Kapton tape windows (2 mm × 10 mm), and XANES data were recorded at 295 K. Low-temperature measurements were not conducted for V XANES because of the low V concentrations in most of the samples (Table 1) and strong absorption of photons at the 5−6 keV energy range by cryostat windows.[22−24] All XANES data were acquired in fluorescence detection mode, using a 30-element germanium array detector (Canberra Industries) at SSRL or a 36-pixel germanium planar detector (Eurisys) at ANBF. At both beamlines, XANES was recorded in the 5250−5700 eV energy range (step sizes: 10 eV below 5450 eV, 0.25 eV at 5450−5525 eV, and 2 eV above 5525 eV). The energy scale was calibrated using a V foil as an internal standard (calibration energy, 5465.0 eV, corresponding to the first peak of the first derivative of the V^0 edge).[43] The possibility of sample photoreduction was generally lower at ANBF than at SSRL because of a lower photon flux, but this also led to lower signal-to-noise ratios.[24] The extents of photoreduction at both beamlines were compared using repeated scans at the same spots for samples **A1** and **B1** (Table 1). As shown in Figure S2 in the SI, a slight photoreduction of V^V-rich samples (an increase in the V^{IV} content by ∼10% in the second XANES scan) was observed at SSRL, and no significant photoreduction was observed at ANBF.[24] In addition, no significant differences between the first and second scans were observed in the XANES of cell samples (recorded at SSRL; see Table 1); a typical example is shown in Figure S2c in the SI. In all cases, only the first scans for each sample were used for data analyses.

The XANES spectra of the model vanadium(V) and -(IV) complexes [**A**−**G** and $(NEt_4)_2[V^V_2(O)_4(met)_2]$ in Chart 1] were recorded previously[21] at ANBF (295 K, fluorescence detection mode), using solid mixtures of the model complexes with boron nitride (BN; ∼1:10 mass ratio). The spectra of **H** and **I** (Chart 1) were resplined[21] from the previously published data[44] for electrochemically generated vanadium(V), -(IV), and -(III) catecholato complexes (10 mM V in DMF, 295 K, fluorescence detection mode). The spectrum of $[V^{IV}O(dedtc)_2]$ (Chart 1) was recorded at SSRL (295 K; fluorescence detection mode; energy range, 5250−6200 eV), using a solid mixture with BN (∼1:10 mass ratio, packed under and argon atmosphere). The spectra of frozen aqueous solutions of V^V-met and V^V-GSH (see above) were recorded at ANBF at 10 K (CryoIndustries reverse cycle liquid-helium cryostat) in fluorescence detection mode at 5250−5700 eV. The XANES spectrum for a complex assigned as $[V^VO(OH)(dtc)_2]$ [dtc = dithiocarbamato(−)] was digitized from the literature data,[45] using *WinDig* software.[46] The spectrum of Na_3VO_4 published in the same work[45] was used for energy calibration.[21]

Calibration, averaging, and splining of XANES data were performed using the *XFit* software package,[47] which uses the *FEFF8* code[48] for EXAFS calculations. The spectra were normalized (using the *Spline* program within the *XFit* package) according to the method of Penner-Hahn and co-workers,[49] to match the tabulated X-ray cross-sectional data[50] for V [in a similar manner to the earlier work on chromium(III) XANES spectra].[11] This normalization technique led to consistent XANES spectra for all of the samples, regardless of the beamline used and the signal-to-noise ratio (see the Results section). Multiple-linear-regression analyses of XANES data were performed using *Origin* software[51] with previously described criteria for a successful fit.[18] Initially, the full set of spectra for model complexes,[21] as well as the data for vanadium(V) and -(IV) thiolato complexes obtained in this work, was used for multiple-linear-regression analyses, but most of the spectral models were rejected computationally during the fitting algorithm because of negative regression coefficients.[18] Principal component analysis (PCA) of XANES spectra[18,52] was performed with *Unscrambler* software.[53]

RESULTS

XANES Spectra of Model Vanadium(V) and -(IV) Thiolato Complexes. Binding of V^V to the thiolato residue in the active sites of PTPs, which leads to changes in the cell signaling, is considered among the likely reasons for both antidiabetic and anticancer activities of vanadium(V) and -(IV) complexes.[1,2,5,13] Cellular thiols, such as GSH, have also been postulated to play a crucial role in cellular reduction of V^V to V^{IV},[54a] although this postulate remains controversial.[36] Recently, GSH was shown to act as a mediator in the reduction of V^V to V^{IV} in ascidians by a specific enzyme, Vanabin2.[54b] Therefore, vanadium(V) and -(IV) thiolato species can be expected to form during the cellular metabolism of medicinal vanadium(V) and -(IV) complexes.[55] Obtaining XANES data for vanadium(V) and -(IV) thiolato models is challenging because of the air and moisture sensitivity of such complexes.[34,35] Our previous library of XANES data[21] included the spectrum of $(NEt_4)_2[V^V_2(O)_4(met)_2]$ (Chart 1).[35] To our knowledge, the only other published XANES spectrum of a vanadium thiolato complex is that of a compound assigned as $[V^VO(OH)(dtc)_2]$,[45] although the details of its characterization are unavailable. Additional vanadium thiolato models used in this work included $[V^{IV}O(dedtc)_2]$ (Chart 1 and Figure S1 in the SI),[34] as well as V^V-met and V^V-GSH species (1:1 vanadium-to-thiol ratio), which were generated in aqueous solution (pH 7.7)[36] and snap-frozen for XAS. A comparison of XANES spectra of these model complexes (Figure 1) shows the unusually low preedge and edge energies for $[V^{IV}O(dedtc)_2]$, as well as a close match of the spectra of V^V-met and V^V-GSH (frozen solutions). On the basis of this resemblance, the solution structure of V^V-GSH (which has not been studied previously)[36] is likely to represent that of a five-coordinate vanadium(V) oxido complex with mixed oxygen/sulfur donors, similar to that of V^V-met (Chart 1).[35,36]

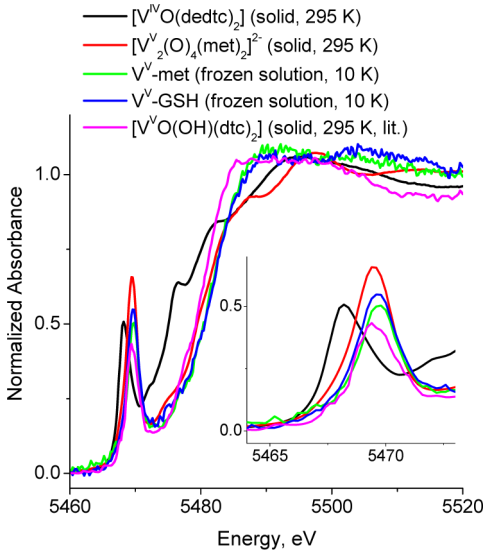

Figure 1. Comparison of the XANES spectra of vanadium(V) and -(IV) thiolato complexes, including the digitized literature data for $[V^VO(OH)(dtc)_2]$.[45] Details of the preparation and XANES data collection for the other complexes are described in the Experimental Section.

Comparison of XANES Spectra of Model and Biological Samples. As reported previously,[22] simple dissolution of **A** or **B** in an aqueous buffer (HBS) at pH 7.40 led to significant changes in the V coordination environment that are reflected in the XANES. In the case of **A**, these changes included a decrease in the intensity of the preedge absorbance

DOI: 10.1021/ic5028948
Inorg. Chem. 2015, 54, 6707−6718

and a change in the postedge shape (**A*** vs **A** in Figure 2a), which were consistent with the formation of a mixture of $[H_2V^VO_4]^-$ and oligomeric vanadates.[6,22,56] In the case of **B**, a marked shift in energy and a decrease in intensity of the preedge absorbance, together with changes in the shapes of the edge and postedge regions (**B*** vs **B** in Figure 2b), were consistent with the formation of six-coordinate vanadium(IV) oxido complexes [most likely $[V^{IV}O(ma)_2(OH_2)]/[V^{IV}O(ma)_2(OH)]^-$, where ma = maltolato(−)].[21,22,57]

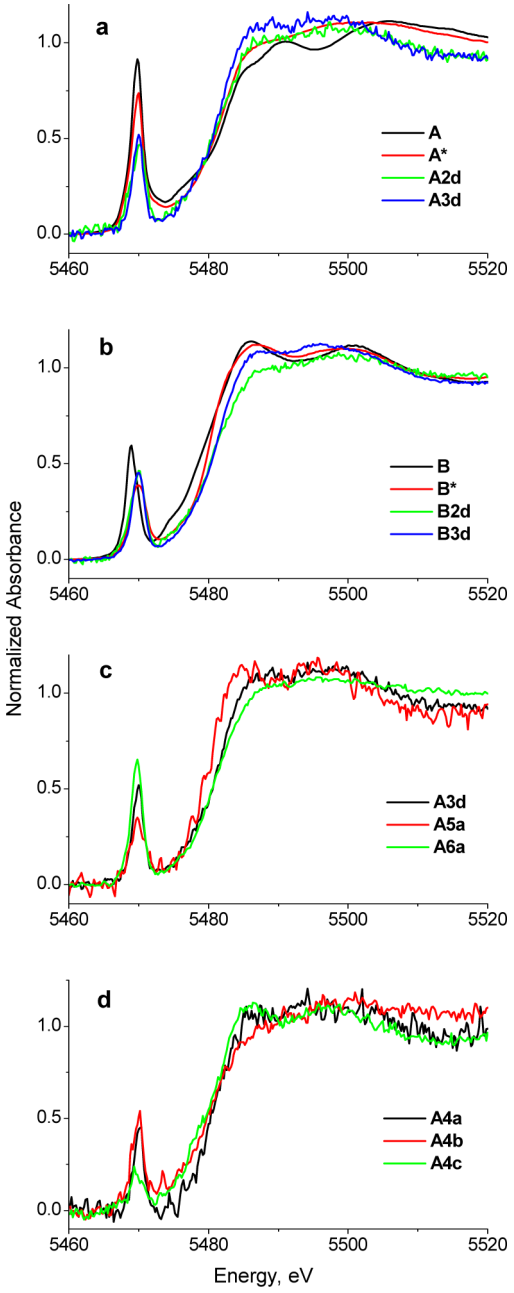

Figure 2. Comparison of the XANES spectra (solids, 295 K) of the initial vanadium complexes (**A** and **B** in Chart 1) and selected reaction products (Table 1): (a) spectra of **A** and its decomposition products in HEPES-buffered saline (**A***), a cell culture medium (**A2d**), and HepG2 cells (**A3d**); (b) spectra of **B** and its decomposition products in HEPES-buffered saline (**B***), a cell culture medium (**B2d**), and HepG2 cells (**B3d**); (c) spectra of decomposition products of **A** in HepG2 cells (**A3d**), in 3T3-L1 adipocytes (**A5a**), and in the corresponding cell culture medium (**A6a**); (d) decomposition products of **A** in intact A549 cells (**A4a**) and in the nuclear (**A4b**) and low-molecular-mass cytoplasmic fractions (**A4c**) of the cell lysate. Detailed comparisons of XANES data for the samples listed in Table 1 are given in Figures S3, S4, and S6 in the SI.

Because all of the samples listed in Table 1 were prepared using cell culture media at the same salinity and pH values as HBS,[37,39,40] the XANES of **A*** and **B*** were used as starting points to follow further speciation changes of **A** or **B** during reactions with HepG2 cells or cell culture media (samples **A2a**−**A2d**, **A3a**−**A3d**, **B2a**−**B2d**, and **B3a**−**B3d** in Table 1). Judging from the values of the preedge absorbance intensities and edge energies,[21] these changes included partial reduction to V^{IV} for **A*** (**A2d** and **A3d** in Figure 2a) and partial oxidation to V^V for **B*** (**B2d** and **B3d** in Figure 2b). Parts a and b of Figure 2 also show significant differences between the XANES of cell and media samples taken from the same treatment (predominantly in the postedge area), which are shown in more detail in Figure S3 in the SI. The differences in the XANES of HepG2 cells treated with either **A** or **B** at each time point (Table 1) did not exceed experimental noise levels (left-hand side column in Figure S4 in the SI). By contrast, there were significant differences between the XANES of cell culture media with added **A** or **B** at 4 or 8 h time points, followed by gradual convergence of the XANES within 24 h (Figure S4 in the SI, right-hand side column). These observations were confirmed by PCA results that showed tight grouping of the cell samples and loose grouping of the media samples (Figure S5 in the SI).

As shown previously,[21−23] a combination of the position and intensity of the preedge peak with the edge energy in the XANES spectra can be used to predict oxidation states and coordination numbers of vanadium(V), -(IV), and -(III) reaction products in biological matrixes. The ranges of these parameters for the samples listed in Table 1 were relatively broad (Figure 3) compared with those for the reaction products of vanadium(V) and -(IV) complexes with blood and its components.[23] Notably, most of the data for the cell samples (Table 1) were tightly grouped in Figure 3a, in agreement with the PCA data (Figure S5 in the SI).

A comparison with the XANES spectroscopic parameters of model vanadium(V) and -(IV) complexes (Figure 3)[21] showed that the biological samples analyzed herein were most likely to contain five- and six-coordinate vanadium(V) and six-coordinate vanadium(IV) complexes. Although relatively high preedge intensities in the XANES of biological samples (Figures 2 and S3 and S4 in the SI) pointed to the predominance of vanadium(V) and -(IV) oxido complexes,[21] the presence of nonoxido species (which are characterized by low preedge XANES peaks)[21,44] as minor components could not be excluded. The XANES parameters for V^V-GSH (in a frozen aqueous solution, **4** in Figure 3a) were consistent with a five-coordinate vanadium(V) complex, while V^V-met and $[V^VO(OH)(dtc)_2]$[45] (**3** and **5** in Figure 3a) were likely to be partially reduced to V^{IV} during the data collection.[24] The XANES parameters of $[V^{IV}O(dedtc)_2]$ (**1** in Figure 3) were very different from those of typical five-coordinate vanadium(IV) complexes,[21] probably because of the electron-donating effect of four sulfur donors[58] and the unusual three-membered-ring structure (Chart 1).

A comparison of the XANES of various mammalian cell lines treated with **A** (samples **A3a**−**A3d**, **A4a**−**A4c**, and **A5a**−**A5c** in Table 1) is shown in Figures 2c,d and S6 in the SI. The XANES of differentiated 3T3-L1 mouse adipocytes, treated with **A** (1.0 mM) for 24 h, suggested a significantly lower average oxidation

DOI: 10.1021/ic5028948
Inorg. Chem. 2015, 54, 6707−6718

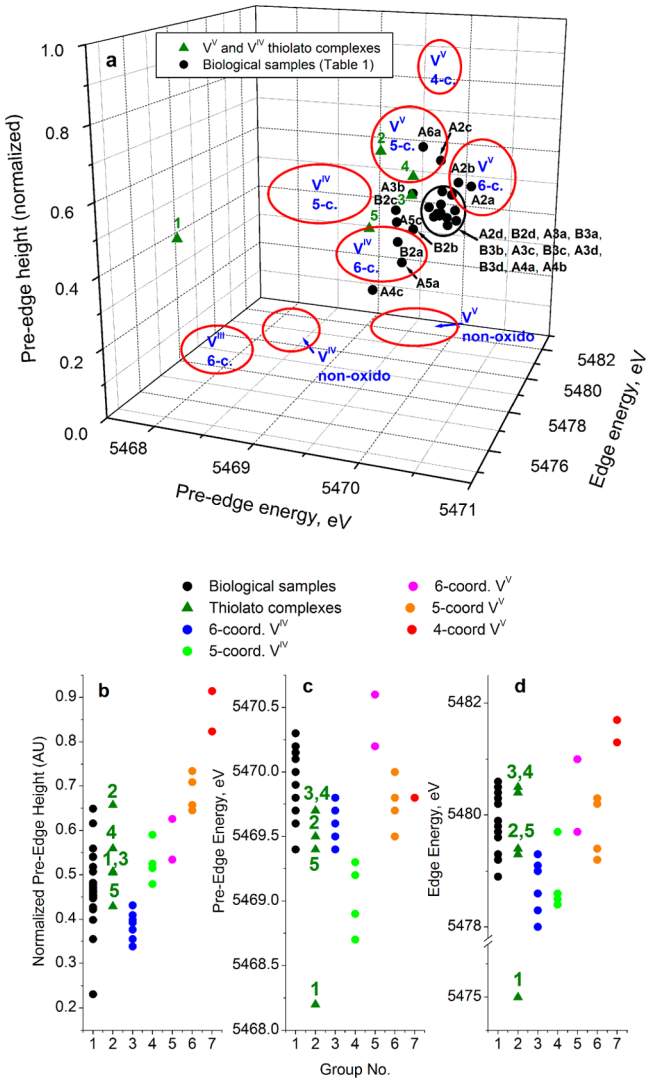

Figure 3. Comparison of the key parameters of XANES spectra (three-dimensional plot, a; its projections on separate axes, b–d).[21] Previously published data[21] for model vanadium(V), -(IV), and -(III) complexes are used (the data for nonoxido complexes are not included into parts b–d). Designations of vanadium(V) and -(IV) thiolato complexes (green triangles; see also Figure 1 and Chart 1): **1** is $[V^{IV}O(dedtc)_2]$; **2** is $(NEt_4)_2[V^V_2(O)_4(met)_2]$; **3** is V^V-met (frozen solution); **4** is V^V-GSH (frozen solution); **5** is $[V^VO(OH)(dtc)_2]$.[45]

state of V compared with those within HepG2 human hepatoma cells (**A5a** vs **A3d** in Figure 1c) or binding to sulfur-donor groups. No significant differences were observed in the XANES of 3T3-L1 adipocytes treated with 0.50, 1.0, or 2.0 mM **A** for 24 h (Figure S6a in the SI). Unlike for all of the other cell samples, the XANES of differentiated 3T3-L1 cells were taken at ANBF (Table 1), which led to low signal-to-noise ratios (Figure S6a in the SI) but also prevented significant photoreduction of the samples.[24] In marked contrast with the differentiated 3T3-L1 cell sample, the XANES of V in the medium from the same treatment showed the predominance of V^V species (**A6a** vs **A5a** in Table 1 and Figure 2c). This difference was more pronounced than the differences in XANES between HepG2 cells and the corresponding media (Figure S3 in the SI). Unlike for HepG2 cells, which were grown and treated in advanced DMEM (containing 2.5 mg L^{-1} of ascorbate),[40] 3T3-L1 cells were grown and treated in DMEM, which did not contain strongly reducing additives (see the Experimental Section),[39] which is a likely explanation for the higher average oxidation state of V reaction products in the latter medium (**A6a** vs **A2d** in Figure 1).[59] Unlike for differentiated 3T3-L1 cells, the XANES of nondifferentiated 3T3-L1 mouse preadipocytes (**A5b** and **A5c** in Table 1) were similar (but not identical, particularly in the postedge area) to those of human cancer cell lines (HepG2 or A549; **A3d** and **A4a** in Table 1), as shown in Figure S6b–d in the SI. All of the XANES data for cultured cells were significantly different from those in red blood cells (RBC; isolated from the reaction of fresh whole rat blood with 1.0 mM **A** for 1–6 h at 310 K),[23] as shown in Figure S6e,f in the SI. In RBC, V^{IV} can bind to the protein residues of the main protein, hemoglobin,[55a] which is likely to produce an environment different from that in the other cells. There were significant differences in V XANES of intact A549 cells and their subcellular fractions (**A4a**–**A4c** in Table 1), particularly for the low-molecular-mass cytoplasmic fraction, which showed a significant reduction in the average oxidation state of V and/or binding to sulfur donors (Figure 2d). The low signal-to-noise ratios in the XANES of A549 cells (Figure 2d) can be explained by the relatively low V content compared with HepG2 cells (Table 1). A comparison of XANES data for the samples listed in Table 1 with the spectrum of V^V-GSH as a possible model of V in the cellular environment[1,2,5,13] (Figure S7 in the SI) showed a relatively close resemblance only in the case of **A4b** (nuclear fraction of A549 cells treated with 1.0 mM **A** for 24 h).

Vanadium Uptake and Speciation in Cultured Mammalian Cells. Multiple-linear-regression analyses of XANES data (Table 1) were performed with the use of a previously developed XANES library of 23 biologically relevant vanadium(V), -(IV), and -(III) complexes,[21] plus the data for vanadium(V) and -(IV) thiolato complexes obtained in this work (Figure 1). The final fits, which are summarized in Figure 4 and Table S1 in the SI, contained the XANES of the reaction products of **A** and **B** with physiological saline at pH 7.40 (designated as **A*** and **B***; see the Experimental Section for details), as well as those of model compounds **C**–**I** (Chart 1). A comparison of the experimental and fitted XANES spectra for all of the samples in Table 1 (except for **A1** and **B1**, which were analyzed elsewhere)[23] is shown in Figure S8 in the SI. Note that vanadium(V) and -(IV) thiolato complexes were excluded from all of the final fits (Figure 4) on the basis of negative correlation coefficients, except for the sample **A4b**, where the fit with 100% V^V-GSH was slightly better than that shown in Figure 4c (see Table S1 and Figure S8 in the SI for details). Attempts to use V^V-GSH in combination with other models in multiple-linear-regression fits were unsuccessful. For most of the samples, except for **B3a**, **B3c**, **B3d**, and **A6a**, the fit residues for the XANES did not significantly exceed the experimental noise levels (Figure S8 in the SI). Differences in the monochromator settings between the data for model complexes (collected mostly at ANBF)[21] and biological samples (collected mostly at SSRL, Table 1) are a likely factor contributing to the fit residues.[60]

In Figure 4a,b, the XANES fitting result for each of the HepG2 cell samples (**A3a**–**A3d** and **B3a**–**B3d**) is shown next to the result for the corresponding cell culture medium sample (**A2a**–**A2d** and **B2a**–**B2d**). The fitting results for A549 and 3T3-L1 cell samples are shown in Figure 4c. Most of the fits in Figure 4 are dominated by five- and six-coordinate vanadium-(V) species (represented by models **E** and **F** in Chart 1) and

DOI: 10.1021/ic5028948
Inorg. Chem. 2015, 54, 6707–6718

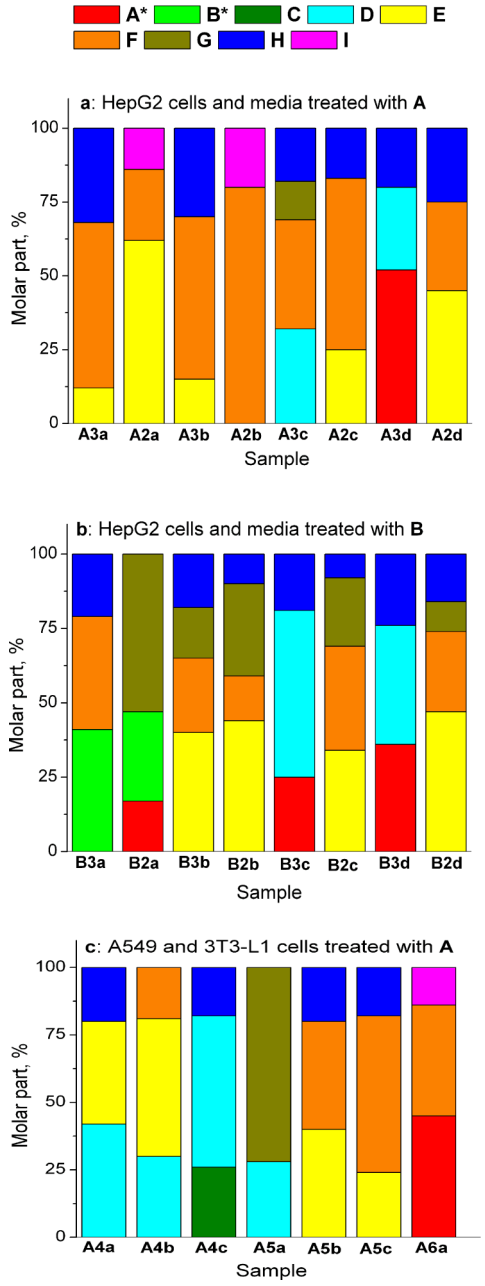

Figure 4. Summary of multiple-linear-regression analysis of XANES data for V-treated cells and cell culture media: (a) reaction products of **A** with HepG2 cells and the corresponding media; (b) reaction products of **B** with HepG2 cells and the corresponding media; (c) reaction products of **A** with A549 and 3T3-L1 cells and the corresponding media. Designations of the samples and models (**A**–**I**) correspond to those in Table 1 and Chart 1 (**A*** and **B*** are the reaction products with HEPES-buffered saline; see the text for details), respectively. Detailed fit results (including the fit errors) are listed in Table S1 in the SI, and overlays of the experimental and fitted XANES data are given in Figure S8 in the SI. Note that an alternative fit for **A4b** included 100% V^V-GSH (Table 1 and Figure S8 in the SI).

six-coordinate vanadium(IV) oxido complexes (models **D** and **G** in Chart 1), in agreement with the data contained within Figure 3. The presence of tetrahedral vanadium(V) oxido species (modeled by **A***)[22,56] after prolonged treatments of HepG2 cells with either **A** or **B** was also suggested by the fitting results (**A3d**, **B3c**, and **B 3d** in Figure 4a,b). Both the cell and medium samples for an early stage of reaction with **B** (4 h of reaction time; **B3a** and **B2a** in Table 1 and Figure 4b) were likely to contain six-coordinate vanadium(IV) oxidomaltolato species (represented by model complex **B***),[22] which dissociated at longer reaction times. Although model compounds **D** and **E** also contain maltolato ligands (Chart 1), the XANES from these models contained within the best fits were more likely to represent V^{IV} and V^V binding to oxygen-donor ligands of the medium (such as carbohydrates, which have mixed carboxylato/alcoholato donor groups, citrate, lactate, or ascorbate)[22b,40,59,61] because these models were also present in the XANES fits for cells and media treated with **A** (Figure 3). The time-dependent V speciation in the reaction products of **B** with the cell culture medium (**B2a**, **B2b**, **B2c**, and **B2d** in Figure 3b) suggests that **B*** initially underwent ligand-exchange reactions to form other V^{IV} species (modeled by a vanadium(IV) citrato complex, **G** in Chart 1), which were then gradually oxidized to V^V species (modeled with **E** and **F** in Chart 1). Because the reaction medium (advanced DMEM) did not contain added citrate[40] (apart from a small amount introduced with serum), the presence of model **G** in the fits was likely due to binding of V^{IV} to other 2-hydroxyacid ligands and carbohydrate ligands with mixed carboxylato/alcoholato donor groups[22b] because vanadium(IV) complexes with simple sugars with 1,2-diolato donor groups are only formed in methanol solutions or from V^V or V^{IV} in aqueous solutions at pH 11–12.[61]

A comparison of the fitting results for **A5a** and **A6a** (differentiated 3T3-L1 cells and the corresponding cell culture media; Table 1 and Figure 4c) showed that these data were fitted entirely by V^{IV} or V^V models for **A5a** or **A6a**, respectively, in agreement with the marked difference in the XANES of these samples (Figure 2c). As for the results for RBC (reported elsewhere),[23] model **G** [vanadium(IV) citrato complex; Chart 1] dominated the fit for **A5a** (Figure 4c), which pointed to V^{IV} binding to both biological oxygen-donor ligands, including carboxylates from complex carbohydrates[22b] and 2-hydroxycarboxylates.[61,62] By contrast with **A5a**, the V speciation obtained in the best fits to the XANES in V^V-treated nondifferentiated 3T3-L1 cells (**A5b** and **A5c** in Figure 4c) was similar to that in typical V^V-treated HepG2 cells (such as **A3a** and **A3b** in Figure 4a). Most of the XANES fits contained significant proportions (8–32 mol %; Table S1 in the SI) of octahedral nonoxidovanadium(IV) and -(V) species, which were modeled with **H** and **I** in Chart 1, although this is likely to be indicative of tyrosinate binding and not six-coordinate nonoxido complexes (see the Discussion section).

The relative amounts of V^V species in each of the samples of HepG2 cells and the corresponding cell culture media, based on the fitting results (Figure 4 and Table S1 in the SI), are shown in Figure 5a (the error bars represent the sums of fit errors for each component; see Table S1 in the SI). The data for cell culture media (black and red lines in Figure 5a) showed the gradual convergence into a mixture of V^V (predominantly) and V^{IV} species, when cells were treated with either V^V (**A**) or V^{IV} (**B**). This result was consistent with the comparison of the XANES spectra at separate time points (Figure S4 in the SI). The prevalence of V^{IV} oxidation to V^V in cell culture media under ambient aerial conditions (Figure 5a) was consistent with the data from isolated blood serum, obtained by either XANES[23] or EPR[63] spectroscopies. The V^V/V^{IV} ratios for HepG2 cell samples were also time-dependent (green and blue lines in Figure 5a), but they did not correlate with the corresponding data for cell culture media, in agreement with

DOI: 10.1021/ic5028948
Inorg. Chem. 2015, 54, 6707–6718

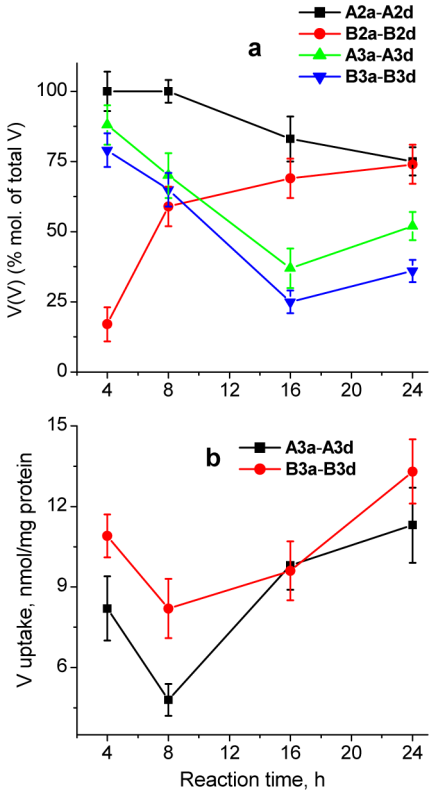

Figure 5. (a) Time-dependent changes in the average oxidation state of V-treated HepG2 cells and the corresponding cell culture media (based on the multiple-linear-regression fits of the XANES data; see Figure 4 and Table S1 in the SI). Error bars represent the sums of fit errors for all of the components; see Table S1 in the SI. (b) Time-dependent V uptake by HepG2 cells (determined by GFAAS). Error bars represent the standard deviations of three measurements, using aliquots of the same sample (see the Experimental Section for details). Designations of the samples correspond to those in Table 1.

the good separation of XANES for these types of samples by PCA (Figure S5 in the SI). For both groups of cell samples (**A3a**–**A3d** and **B3a**–**B3d** in Table 1 and Figure 5a), the highest relative V^{IV} content was observed after 16 h of treatment. The XANES data for the cell samples treated with **A** consistently showed slightly higher average oxidation states of V compared with those in **B**-treated cell samples (Figure 5a), but the significance of this difference is uncertain, given that the best fits to the XANES for the latter group of samples had significantly higher residuals (Figure S8 in the SI). On the other hand, the consistent fitting results obtained for both cell groups (green and blue lines in Figure 5a) indicated that the XANES fits for **B3a**–**B3d** were still reliable, despite the relatively large residues (Figure S8 in the SI). Measurements of the V content in HepG2 cell samples (Table 1) resulted in similar time dependences for V uptake in cells treated with either **A** or **B**, with a decrease between the 4 and 8 h treatments, followed by increases for the 16 and 24 h treatments (Figure 5b).

DISCUSSION

Effects of the Medium on Intracellular Uptake and Speciation. The reactivity of transition-metal complexes in cell culture media can significantly complicate the interpretation of their biological activities in cell cultures.[5,19] For instance, multiple-linear-regression analyses of XANES data (Figures 4 and 5a) indicated that tetrahedral vanadate (**A**) was converted into a mixture of five- and six-coordinate vanadium(V) species within 4 h of reaction with advanced DMEM[40] (containing 2 vol % fetal calf serum) at 310 K, which was followed by the partial reduction of V^{V} to V^{IV} within 24 h at 310 K (samples **A2a**–**A2d** in Figure 4a). By contrast, reaction of **A** with regular DMEM[39] (containing 10 vol % fetal calf serum) for 24 h at 310 K led entirely to vanadium(V) species (four-, five-, and six-coordinate; sample **A6a** in Figure 4c), which shows that small differences in cell culture media (such as the presence of ascorbate in advanced DMEM)[40,59] can have a profound effect on V speciation. There were marked differences between the reaction products of **A** or **B** with advanced DMEM at 4–8 h reaction times (samples **A2a**, **A2b**, **B2a**, and**B2b** in Figure 4a,b), which led to significantly higher V^{IV}/V^{V} ratios in the reaction products of **B** in cell culture media (Figure 5a) and also to significantly higher cellular V uptake compared with the treatments with **A** (Figure 4b). These data support the hypothesis[64] that antidiabetic vanadium(IV) complexes (such as **B**), or their reaction products that at least partially retained the original ligands, entered cells by passive diffusion (unlike for **A**, which was assumed to enter through anion channels).[1,5,7] The differences in V speciation in the reaction products of **A** or **B** with a cell culture medium gradually disappeared after 16–24 h of reaction (**A2c**, **A2d**, **B2c**, and **B2d** in Figure 4a,b), resulting in products that contained ~75% V^{V} (represented by models **E** and **F** in Chart 1) and ~25% V^{IV} (modeled by **G** and **H** in Chart 1). The nitrogen-donor ligand in **F** is likely to model the binding of vanadium(V) to imidazole side chains of proteins.[55] Similar speciation was observed previously for the reaction products of **A** or **B** with undiluted blood serum or plasma, but convergence of the products occurred within 1 h at 310 K.[23] This difference in the reaction rates suggests that serum components play a significant role in the reactivity of vanadium complexes in the cell culture medium (which contained 2 vol % serum in this study). Convergence of the reaction products of typical vanadium(V) and -(IV) complexes in a cell culture medium within 24 h at 310 K (Figures 4a,b and 5a) was consistent with similar results of cell assays that were used to test the antidiabetic activities of various vanadium(V) and -(IV) complexes (typical cell treatment times were 24–72 h).[10] Clearly, these results highlight the variability in speciation that could arise depending on whether these prodrugs were dissolved in media or buffer before adding them to the cell culture and the time they were dissolved in stock solutions prior to adding aliquots to the medium. This is important because the efficacy and toxicity can clearly change with time as both the extracellular and intracellular speciation changes. As such, caution has to be exercised in performing assays that most strongly resemble the in vivo conditions that change speciation in the gastrointestinal tract and, subsequently, the circulating blood after oral administration in order to obtain the most biologically relevant conditions for evaluating potential in vivo activities of the prodrugs.[5,19,22,23]

V Speciation in Cells. The differences in V speciation in HepG2 cells treated with either **A** or **B** for 4–8 h (**A3a**, **A3b**, **B3a**, and**B3b** in Figure 4a,b) were much less pronounced than those in the corresponding cell culture medium samples. The data contained within Figure 5a showed that similar mixtures of vanadium(V) and -(IV) species rapidly formed in cells regardless of the prevalent V oxidation state present in the medium, which points to the existence of active cellular metabolic pathways that include both oxidation of V^{IV} and reduction of V^{V}. This is similar to the intracellular redox

DOI: 10.1021/ic5028948
Inorg. Chem. 2015, 54, 6707–6718

recycling postulated for Cr(III) and its higher oxidation states in its anti-diabetic activity.[5] The V^{IV}/V^{V} ratios in the cells increased with time for 4−16 h treatment times, followed by a slight increase in the cellular V^{V} content at 24 h (green and blue lines in Figure 5a). All of the XANES fits for V-treated HepG2 cells included significant proportions (18−32 mol %; Figure 3 and Table S1 in the SI) of model **H** [Chart 1; a nonoxidovanadium(IV) complex], which is likely to represent (at least partially) the vanadium(IV) binding to phenolato (tyrosine) residues of proteins[23] and not the presence of nonoxido species per se. An alternative explanation for the presence of model **H** in the fits is the formation of vanadium(IV) thiolato species[54] that are not adequately described by the only vanadium(IV) thiolato model used ($[V^{IV}O(dedtc)_2]$ in Chart 1 and Figure 1). No significant contributions of vanadium(V) or -(IV) thiolato models (Figure 1) were observed in the fits for intact cell samples (Figure 4) at the high V concentrations used in this work, but their contributions are likely to increase when more physiologically relevant V concentrations are used.[1,65] Prolonged reaction times led to the appearance of model **A*** [highly reactive tetrahedral vanadium(V) oxido species][22,56] in the best XANES fits for the cell samples (**A3d**, **B3c**, and **B3d** in Figure 4a,b), which may indicate that the protective capacity of the cell had been exhausted (in agreement with visible changes in the cell morphology at this time).[66] Biphasic curves of cellular V uptake in HepG2 cells (Figure 5b), which were consistent with the literature data on the time-dependent uptake of **A** by cultured mammalian cells,[67] also pointed to the presence of a protective mechanism against V toxicity, which led to partial removal of V from cells between 4 and 8 h of treatment (Figure 5b).

The XANES data for differentiated 3T3-L1 adipocytes treated with **A** (**A5a** in Figure 4c) pointed to a higher V^{V}-reducing capacity of these cells compared with the other studied cell lines, including nondifferentiated 3T3-L1 preadipocytes (**A5b** and **A5c** in Figure 4c). The V^{V}-reducing capacity of adipocytes was similar to that of RBC.[23] The prevalence of vanadium(IV) species was also found in the low-molecular-mass cytoplasmic fraction of A549 cells treated with **A** (**A4c** in Figure 4c), while mixtures of vanadium(V) and -(IV) species were present both in the intact cells (**A4a**) and in the nuclear fraction (**A4b**). These data indicated that V^{V} reduction to V^{IV} was likely to have occurred in the cytoplasm, while the increase in the proportion of V^{V} after prolonged treatment times (Figure 5a) was likely to have been due to V^{V} uptake by the cell nucleus, which coincided with changes in the cell morphology due to V toxicity. By contrast, a recent study of V speciation in the lysates of HepG2 cells after treatment with **B**, which was performed by chromatography and mass spectrometry techniques, pointed to the formation of predominantly vanadium(V) low-molecular-mass species (assigned as a divanadate phosphate derivative).[26] Although all the procedures used in cell lysis and fraction separation can introduce changes to metal ion speciation,[18] the lengthy chromatographic procedures[26] were more likely to lead to V(IV) oxidation to V(V) by aerial oxygen.[63]

The XANES fits for subcellular fractions of A549 cells (**A4b** and **A4c** in Figure 4c) point to the presence of an active mechanism of V^{V} transport to the cell nucleus. This mechanism is likely to involve electrostatic binding of negatively charged vanadates to the positively charged side chains of histone proteins, as was observed for chromate and is well-known for phosphate and sulfate.[68] Notably, a good fit of the XANES data for nuclear V^{V} was also obtained using the V^{V}-GSH model only (Figure 1 and Table S1 and Figures S7 and S8 in the SI), which may point to V^{V} binding to thiol-rich zinc finger proteins[69] in the nucleus. However, no definitive choice can be made between the two alternative XANES fits for sample **A4b** (Figure 4c and Figure S8 and Table S1 in the SI) at this stage. Once within the nucleus, vanadate can also affect both translation and transcription by binding to various proteins,[70] and it is also well-known to inhibit RNases.[71] Thus, it has the potential to change the phenotype and/or the phase of the cell and/or lead to cell toxicity. These factors combined are consistent with the change in the cell morphology and are likely to have important implications in both the antidiabetic and anticancer properties of V.

The V concentrations (typically 1.0 mM) used were visibly toxic for the cells at >8 h treatments, but the use of lower V concentrations was difficult because of the X-ray fluorescence detection sensitivity limits.[19] However, a treatment of 3T3-L1 cells (nondifferentiated) either with 1.0 mM **A** for 8 h or with 0.10 mM **A** (a nontoxic concentration) for 72 h resulted in nearly identical V speciation (samples **A5b** and **A5c** in Figures 3c and S5b in the SI). Clearly, cell treatments with V concentrations that are likely to form in the blood during the treatments with V antidiabetics (low micromolar levels)[1,65] would be preferable, but these conditions did not produce detectable V levels in bulk cell samples (data not shown). This problem is being addressed by the application of X-ray fluorescent mapping in conjunction with XANES spectroscopy of single cultured mammalian cells at the Advanced Photon Source, Argonne, IL.[19] This technique increased the sensitivity of V detection and enabled the determination of the relative concentrations, redox states, and coordination environments of vanadium in different cellular compartments (McLeod, A. I.; Aitken, J. B.; Levina, A.; Lay, P. A., to be submitted). Another limitation of these studies was the need to use freeze-dried samples because of a relatively low sensitivity to the metal ion and high absorption background of the XANES spectroscopy at 5−6 eV.[22−24] However, the consistent time-dependent changes for the reactions of either **A** or **B** in cell culture media or in HepG2 cells (Figures 4a,b and 5a) strongly indicated that the average oxidation states and coordination environments of vanadium in freeze-dried samples correlated with those in the corresponding reaction solutions.

CONCLUSIONS

In summary, typical antidiabetic vanadium(V) and -(IV) complexes, **A** and **B** (Chart 1),[1,5,7] underwent profound transformations in cell culture media, and the resultant products were further metabolized by cultured mammalian cells, as illustrated in Scheme 1, in the interactions with either HepG2 cells (a) or mature 3T3-L1 adipocytes (b) for 24 h at 310 K. These transformations included both V^{V} reduction and V^{IV} oxidation (Figures 4 and 5a). The easy interconversions of vanadium(IV) and -(V) species in the cells and in cell culture media (as well as in gastrointestinal media and in the blood)[22,23,63] also meant that the attribution of different biological activities to different oxidation states of vanadium in the literature[72] is likely to be unreliable. The results of XANES spectroscopic studies presented herein support the roles of vanadium(V) species, including vanadium(V) peroxido complexes that form during the reactions of vanadium(V) or -(IV) metabolism products with endogenous H_2O_2,[73] as reactive intermediates responsible for both antidiabetic and cytotoxic

DOI: 10.1021/ic5028948
Inorg. Chem. 2015, 54, 6707−6718

Scheme 1. Typical Proposed Speciation of V^{V} and V^{IV} in Cultured Cells and Cell Culture Media, Based on the Results of Multiple-Linear-Regression Fits of XANES Data (Figure 4 and Table S1 in the SI)[a]

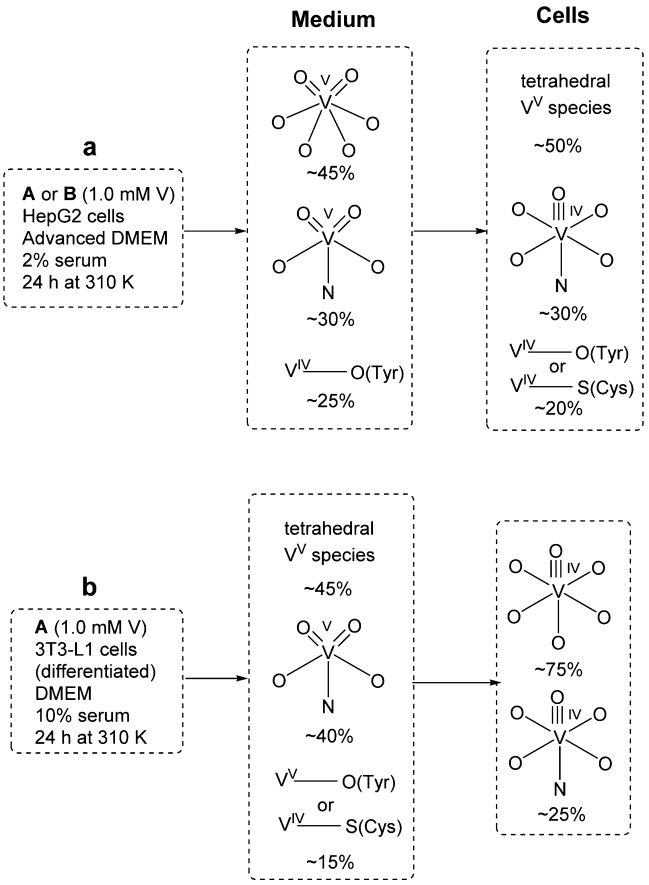

[a]See the note in Chart 1 on actual bond orders in vanadium(IV) and -(V) oxido complexes.[38] The presented data include the samples **A2d**, **B2d**, **A3d**, and **B3d** for part a and the samples **A5a** and **A6a** for part b (designations correspond to those in Table 1 and Figure 4).

activities of vanadium(V) and -(IV) complexes.[5] Importantly, XANES spectroscopic studies revealed for the first time the capacity of intact mammalian cells to generate and maintain vanadium(V) when treated with vanadium(IV) complexes (samples **B3a** vs **B2a** in Figures 4b and 5a). The likely cellular targets of vanadium(V) include a variety of phosphatase enzymes, including PTPs, ATPases in the cytoplasm and nucleases in the cell nucleus, and RNases, which affect both cell signaling and DNA expression.[56] Relatively mild changes in the activity of these enzymes would enhance cellular glucose metabolism, while more profound changes would lead to cell death through apoptosis,[5,74] which is likely to lead to the observed anticancer effects of vanadium.[4,7] Previous studies that were performed mostly by EPR spectroscopy had focused on the reduction of V^{V} to V^{IV} by cells (usually RBC).[54,55,75] In agreement with the published results, the present study has also shown the high capacity of cultured cells to take up V^{V} from cell culture medium and to reduce it to V^{IV}, particularly in 3T3-L1 adipocytes (samples **A5a** vs **A6a** in Figure 4c). The distinct V biochemistry in mature 3T3-L1 adipocytes (**A5a** in Figure 4) compared to other cell lines, including 3T3-L1 preadipocytes, is consistent with the crucial role of these cells in insulin-dependent glucose and fat metabolism.[31] Reported effects of exogenous V treatments in 3T3-L1 adipocytes include the enhancement of insulin receptor signaling,[25a] increased fat production,[25c] and activation of Akt signaling pathways.[25e] The present data may also point to an endogenous role of V in these cells, although no conclusive evidence of V essentiality in mammals has been found as yet.[7]

■ ASSOCIATED CONTENT

Supporting Information

Details of the synthesis and characterization (including EXAFS data analysis) of $[V^{IV}O(dedtc)_2]$, assessment of the photoreduction of biological vanadium(V) and -(IV) samples at ANBF and SSRL, detailed comparison of XANES spectra of biological samples listed in Table 1 and their overlays with the spectrum of V^{V}-GSH, results of PCA of the XANES data for V-treated HepG2 cells and the corresponding cell culture media, a table of detailed results of multiple-linear-regression analyses of XANES data, and overlays of experimental and fitted XANES spectra for the samples listed in Table 1. This material is available free of charge via the Internet at http://pubs.acs.org.

■ AUTHOR INFORMATION

Corresponding Author

*E-mail: peter.lay@sydney.edu.au.

Notes

The authors declare no competing financial interest.

■ ACKNOWLEDGMENTS

The research was supported by Australian Research Council (ARC) Discovery Grants DP0208409, DP0774173, DP0984722, DP1095310, and DP130103566, ARC Professorial Fellowship Grants DP0208409 and DP0984722 to P.A.L., and an ARC LIEF grant (LE0346515) for the 36-pixel Ge detector at ANBF. XAS was performed partially at ANBF with support from the Australian Synchrotron Research Program (ASRP), which is funded by the Commonwealth of Australia under the Major National Research Facilities program and partially at SSRL, which is operated by the Department of Energy, Office of Basic Energy Sciences. The SSRL Biotechnology Program is supported by the National Institutes of Health, National Center for Research Resources, Biomedical Technology Program, and by the Department of Energy, Office of Biological and Environmental Research. The research at SSRL was also supported by the ASRP. We thank Drs. Garry Foran, James Hester, Celesta Fong, and Michael Cheah for assistance with XAS experiments at ANBF and Matthew Latimer for those at SSRL. We also acknowledge the facilities as well as scientific and technical assistance from staff in the Australian Centre for Microscopy and Microanalysis at The University of Sydney.

■ REFERENCES

(1) Thompson, K. H.; Orvig, C. *J. Inorg. Biochem.* **2006**, *100*, 1925−1935.
(2) Zhang, M.; Zhou, M.; Van Etten, R. L.; Stauffacher, C. V. *Biochemistry* **1997**, *36*, 15−23.
(3) Srivastava, A. K.; Mehdi, M. Z. *Diabetic Med.* **2005**, *22*, 2−13.
(4) Barrio, D. A.; Etcheverry, S. B. *Curr. Med. Chem.* **2010**, *17*, 3632−3642.
(5) Levina, A.; Lay, P. A. *Dalton Trans.* **2011**, *40*, 11675−11686.
(6) Willsky, G. R.; Chi, L.-H.; Godzala, M.; Kostyniak, P. J.; Smee, J. J.; Trujillo, A. M.; Alfano, J. A.; Ding, W.; Hu, Z.; Crans, D. C. *Coord. Chem. Rev.* **2011**, *255*, 2258−2269.

DOI: 10.1021/ic5028948
Inorg. Chem. 2015, 54, 6707−6718

(7) (a) Rehder, D. *Future Med. Chem.* **2012**, *4*, 1823−1837. (b) Rehder, D. *Dalton Trans.* **2013**, *42*, 11749−11761.
(8) Setyawati, I. A.; Thompson, K. H.; Yuen, V. G.; Sun, Y.; Battell, M.; Lyster, D. M.; Vo, C.; Ruth, T. J.; Zeisler, J. H.; McNeill, J. H.; Orvig, C. *J. Appl. Physiol.* **1998**, *84*, 569−575.
(9) Thompson, K. H.; Liboiron, B. D.; Sun, Y.; Bellman, K. D. D.; Setyawati, I. A.; Patrick, B. O.; Karunaratne, V.; Rawji, G.; Wheeler, J.; Sutton, K.; Bhanot, S.; Cassidy, C.; McNeill, J. H.; Yuen, V. G.; Orvig, C. *J. Biol. Inorg. Chem.* **2003**, *8*, 66−74.
(10) Rehder, D.; Costa Pessoa, J.; Geraldes, C. F. G. C.; Castro, M. C. A.; Kabanos, T.; Kiss, T.; Meier, B.; Micera, G.; Pettersson, L.; Rangel, M.; Salifoglou, A.; Turel, I.; Wang, D. *J. Biol. Inorg. Chem.* **2002**, *7*, 384−396.
(11) Nguyen, A.; Mulyani, I.; Levina, A.; Lay, P. A. *Inorg. Chem.* **2008**, *47*, 4299−4309.
(12) Yoshikawa, Y.; Sakurai, H.; Crans, D. C.; Micera, G.; Garribba, E. *Dalton Trans.* **2014**, *43*, 6965−6972.
(13) Peters, K. G.; Davis, M. G.; Howard, B. W.; Pokross, M.; Rastogi, V.; Diven, C.; Greis, K. D.; Eby-Wilkens, E.; Maier, M.; Evdokimov, A.; Soper, S.; Genbauffe, F. *J. Inorg. Biochem.* **2003**, *96*, 321−330.
(14) Costa Pessoa, J.; Tomaz, I. *Curr. Med. Chem.* **2010**, *17*, 3701−3738.
(15) Crans, D. C.; Woll, K. A.; Prusinskas, K.; Johnson, M. D.; Norkus, E. *Inorg. Chem.* **2013**, *52*, 12262−12275.
(16) Sanna, D.; Micera, G.; Garribba, E. *Inorg. Chem.* **2013**, *52*, 11975−11985.
(17) Costa Pessoa, J.; Gonçalves, G.; Roy, S.; Correia, I.; Mehtab, S.; Santos, M. F. A.; Santos-Silva, T. *Inorg. Chim. Acta* **2014**, *420*, 60−68.
(18) Levina, A.; Harris, H. H.; Lay, P. A. *J. Am. Chem. Soc.* **2007**, *129*, 1065−1075.
(19) Aitken, J. B.; Levina, A.; Lay, P. A. *Curr. Top. Med. Chem.* **2011**, *11*, 553−571.
(20) Hummer, A. A.; Rompel, A. *Metallomics* **2013**, *5*, 597−614.
(21) (a) Levina, A.; McLeod, A. I.; Lay, P. A. *Chem.—Eur. J.* **2014**, *20*, 12056−12060. (b) Liu, M.; Lim, Z. J.; Gwee, Y. Y.; Levina, A.; Lay, P. A. *Angew. Chem., Int. Ed. Engl.* **2010**, *49*, 1661−1664.
(22) (a) Levina, A.; McLeod, A. I.; Kremer, L. E.; Aitken, J. B.; Glover, C. J.; Johannessen, B.; Lay, P. A. *Metallomics* **2014**, *6*, 1880−1888. (b) Kremer, L. E.; McLeod, A. I.; Aitken, J. B.; Levina, A.; Lay, P. A. *J. Inorg. Biochem.*, in press, DOI: 10.1016/j.jinorgbio.2015.03.016.
(23) Levina, A.; McLeod, A. I.; Gasparini, S.; De Silva, W. G. M.; Aitken, J. B.; Glover, C. J.; Johannessen, B.; Lay, P. A., submitted.
(24) George, G. N.; Pickering, I. J.; Pushie, M. J.; Nienaber, K.; Hackett, M. J.; Ascone, I.; Hedman, B.; Hodgson, K. O.; Aitken, J. B.; Levina, A.; Glover, C.; Lay, P. A. *J. Synchrotron Radiat.* **2012**, *19*, 875−886.
(25) (a) Ou, H.; Yan, L.; Mustafi, D.; Makinen, M. W.; Brady, M. J. *J. Biol. Inorg. Chem.* **2005**, *10*, 874−886. (b) Basuki, W.; Hiromura, M.; Adachi, Y.; Tayama, K.; Hattori, M.; Sakurai, H. *Biochem. Biophys. Res. Commun.* **2006**, *349*, 1163−1170. (c) Shukla, R.; Bhonde, R. R. *Biometals* **2008**, *21*, 205−210. (d) Zhao, P.; Yang, X. *Metallomics* **2013**, *5*, 836−843. (e) Liu, J. C.; Yu, Y.; Wang, G.; Wang, K.; Yang, X. G. *Metallomics* **2013**, *5*, 813−820.
(26) Nischwitz, V.; Davies, J. T.; Marshall, D.; González, M.; Gómez Ariza, J. L.; Goenaga-Infante, H. *Metallomics* **2013**, *5*, 1685−1697.
(27) HepG2 human hepatocellular carcinoma cell line; ATCC no. HB-8065.
(28) Guo, L.; Dial, S.; Shi, L.; Branham, W.; Liu, J.; Fang, J.-L.; Green, B.; Deng, H.; Kaput, J.; Ning, B. *Drug Metab. Dispos.* **2011**, *39*, 528−538.
(29) Moore, M. C.; Coate, K. C.; Winnick, J. J.; An, Z.; Cherrington, A. D. *Adv. Nutr.* **2012**, *3*, 286−294.
(30) 3T3-L1 mouse fibroblasts (pre-adipocytes); ATCC no. CL-173.
(31) Guiherme, A.; Virbasius, J. V.; Puri, V.; Czech, M. P. *Nat. Rev. Mol. Cell. Biol.* **2008**, *9*, 367−377.
(32) A549 human lung carcinoma cell line; ATCC no. CCL-185.
(33) Caravan, P.; Gelmini, L.; Glover, N.; Herring, F. G.; Li, H.; McNeill, J. H.; Rettig, S. J.; Setyawati, I. A.; Shuter, E.; Sun, Y.; Tracey, A. S.; Yuen, V. G.; Orvig, C. *J. Am. Chem. Soc.* **1995**, *117*, 12759−12770.
(34) McCormick, B. J. *Inorg. Chem.* **1968**, *7*, 1965−1970.
(35) Bhattacharyya, S.; Batchelor, R. J.; Einstein, F. W. B.; Tracey, A. S. *Can. J. Chem.* **1999**, *77*, 2088−2094.
(36) Crans, D. C.; Zhang, B.; Gaidamauskas, E.; Keramidas, A. D.; Willsky, G. R.; Roberts, C. R. *Inorg. Chem.* **2010**, *49*, 4245−4256.
(37) HEPES-buffered saline. Cold Spring Harbor Protocols, 2006, doi: 10.1101/pdb.rec8786.
(38) (a) Ballhausen, C. J.; Gray, H. B. *Inorg. Chem.* **1962**, *1*, 111−122. (b) Winkler, J. R.; Gray, H. B. *Struct. Bonding (Berlin)* **2012**, *142*, 17−28.
(39) Dulbecco's modified Eagle's medium (DMEM), high glucose, catalog no. 10938-025, Invitrogen Corp.
(40) Advanced DMEM, catalog no. 12491-015, Invitrogen Corp.
(41) Govers, R.; Coster, A. C. F.; James, D. E. *Mol. Cell. Biol.* **2004**, *24*, 6456−6466.
(42) Bio-Rad Protein Assay (technical bulletin), catalog no. 500-0002, Bio-Rad Laboratories.
(43) Thompson, A. C.; Attwood, D. T.; Gullikson, E. M.; Howells, M. R.; Kortright, J. B.; Robinson, A. L.; Underwood, J. H.; Kim, K.-J.; Kirz, J.; Lindau, I.; Pianetta, P.; Winick, H.; Wil-liams, G. P.; Scofield, J. H. *X-Ray Data Booklet*, 2nd ed.; University of California: Berkeley, CA, 2001.
(44) Milsmann, C.; Levina, A.; Harris, H. H.; Foran, G. J.; Turner, P.; Lay, P. A. *Inorg. Chem.* **2006**, *45*, 4743−4754.
(45) Weidemann, C.; Rehder, D.; Kuetgens, U.; Hormes, J.; Vilter, H. *Chem. Phys.* **1989**, *136*, 405−412.
(46) Lovy, D. *WinDig*, University of Geneva: Geneva, Switzerland, 1996.
(47) (a) Ellis, P. J.; Freeman, H. C. *J. Synchrotron Radiat.* **1995**, *2*, 190−195. (b) *XFit for Windows, beta-version*; Australian Synchrotron Research Program: Sydney, Australia, 2004.
(48) Ankudinov, A. L.; Ravel, B.; Rehr, J. J.; Conradson, S. D. *Phys. Rev. B* **1998**, *58*, 7565−7576.
(49) Weng, T.-C.; Waldo, G. S.; Penner-Hahn, J. E. *J. Synchrotron Radiat.* **2005**, *12*, 506−510.
(50) McMaster, W. H.; Kerr Del Grande, N.; Mallett, J. H.; Hubbell, J. H. *Compilation of X-ray Cross Sections*; Lawrence Livermore National Laboratory: Livermore, CA, 1969.
(51) *Microcal Origin*, version 6.0; Microcal Software Inc.: Northampton, MA, 1999.
(52) Ressler, T.; Wong, J.; Roos, J.; Smith, I. L. *Environ. Sci. Technol.* **2000**, *34*, 950−958.
(53) *Unscrambler*, version 9.5; Camo Process AS: Oslo, Norway, 2005.
(54) (a) Garner, M.; Reglinski, J.; Smith, W. E.; McMurray, J.; Abdullah, I.; Wilson, R. *J. Biol. Inorg. Chem.* **1997**, *2*, 235−241. (b) Yamamoto, S.; Matsuo, K.; Michibata, H.; Ueki, T. *Inorg. Chim. Acta* **2014**, *420*, 47−52.
(55) (a) Sanna, D.; Serra, M.; Micera, G.; Garribba, E. *Inorg. Chem.* **2014**, *53*, 1449−1464. (b) Sanna, D.; Serra, M.; Micera, G.; Garribba, E. *Inorg. Chim. Acta* **2014**, *420*, 75−84.
(56) Crans, D. C.; Smee, J. J.; Gaidamauskas, E.; Yang, L. *Chem. Rev.* **2004**, *104*, 849−902.
(57) Hanson, G. R.; Sun, Y.; Orvig, C. *Inorg. Chem.* **1996**, *35*, 6507−6512.
(58) (a) Levina, A.; Zhang, L.; Lay, P. A. *Inorg. Chem.* **2003**, *42*, 767−784. (b) Levina, A.; Lay, P. A. *Inorg. Chem.* **2004**, *43*, 324−335.
(59) (a) Song, B.; Aebischer, N.; Orvig, C. *Inorg. Chem.* **2002**, *41*, 1357−1364. (b) Wilkins, P. C.; Johnson, M. D.; Holder, A. A.; Crans, D. C. *Inorg. Chem.* **2006**, *45*, 1471−1479.
(60) Chaurand, P.; Rose, J.; Briois, V.; Salome, M.; Proux, O.; Nassif, V.; Olivi, L.; Susini, J.; Hazemann, J.-L.; Bottero, J.-Y. *J. Phys. Chem. B* **2007**, *111*, 5101−5110.
(61) Baran, E. J. *J. Inorg. Biochem.* **2009**, *103*, 547−553.
(62) (a) Hambley, T. W.; Judd, R. J.; Lay, P. A. *Inorg. Chem.* **1992**, *31*, 343−345. (b) Barr-David, G.; Hambley, T. W.; Irwin, J. A.; Judd, R. J.; Lay, P. A.; Martin, B. D. *Inorg. Chem.* **1992**, *31*, 4906−4908.

DOI: 10.1021/ic5028948
Inorg. Chem. 2015, 54, 6707−6718

(63) Chasteen, N. D.; Grady, J. K.; Holloway, C. E. *Inorg. Chem.* **1986**, *25*, 2754−2760.
(64) Crans, D. C.; Trujillo, A. M.; Pharazyn, P. S.; Cohen, M. D. *Coord. Chem. Rev.* **2011**, *255*, 2178−2192.
(65) Willsky, G. R.; Halvorsen, K.; Godzala, M. E.; Chi, L.-H.; Most, M. J.; Kaszynski, P.; Crans, D. C.; Goldfine, A. B.; Kostyniak, P. J. *Metallomics* **2013**, *5*, 1491−1502.
(66) Harris, H. H.; Levina, A.; Dillon, C. T.; Mulyani, I.; Lai, B.; Cai, Z.; Lay, P. A. *J. Biol. Inorg. Chem.* **2005**, *10*, 105−118.
(67) Bracken, W. M.; Sharma, R. P.; Elsner, Y. Y. *Cell Biol. Toxicol.* **1985**, *1*, 259−268.
(68) Levina, A.; Harris, H. H.; Lay, P. A. *J. Biol. Inorg. Chem.* **2006**, *11*, 225−234.
(69) Levina, A.; Bailey, A. M.; Champion, G.; Lay, P. A. *J. Am. Chem. Soc.* **2000**, *122*, 6208−6216.
(70) Zhang, Z.; Gao, N.; He, H.; Huang, C.; Luo, J.; Shi, X. *Mol. Cell. Biochem.* **2004**, *255*, 227−237.
(71) Berger, S. L. *Methods Enzymol.* **1987**, *152*, 227−234.
(72) (a) Li, J.; Elberg, G.; Crans, D. C.; Shechter, Y. *Biochemistry* **1996**, *35*, 8314−8318. (b) Lampronti, I.; Bianchi, N.; Borgatti, M.; Fabbri, E.; Vizziello, L.; Khan, M. T. H.; Ather, A.; Brezena, D.; Tahir, M. M.; Gambari, R. *Oncol. Rep.* **2005**, *14*, 9−15. (c) Kawabe, K.; Yoshikawa, Y.; Adachi, Y.; Sakurai, H. *Life Sci.* **2006**, *78*, 2860−2866. (d) Xie, M.; Chen, D.; Zhang, F.; Willsky, G. R.; Crans, D. C.; Ding, W. *J. Inorg. Biochem.* **2014**, *136*, 47−56.
(73) (a) Huyer, G.; Liu, S.; Kelly, J.; Moffat, J.; Payette, P.; Kennedy, B.; Tsaprailis, G.; Gresser, M. J.; Ramachandran, C. *J. Biol. Chem.* **1997**, *272*, 843−851. (b) García-Vicente, S.; Yraola, F.; Marti, L.; González-Muños, E.; García-Barrado, M. J.; Cantó, C.; Abella, A.; Bour, S.; Artuch, R.; Sierra, C.; Brandi, N.; Carpéné, C.; Moratinos, J.; Camps, M.; Palacín, M.; Testar, X.; Gumà, A.; Albericio, F.; Royo, M.; Mian, A.; Zorzano, A. *Diabetes* **2007**, *56*, 486−493.
(74) (a) Morinville, A.; Maysinger, D.; Shaver, A. *Trends Pharmacol. Sci.* **1998**, *19*, 452−460. (b) Hulley, P.; Davison, A. *J. Trace Elem. Exp. Med.* **2003**, *16*, 281−290. (c) Goncalves, A. P.; Videira, A.; Soares, P.; Maximo, V. *Life Sci.* **2011**, *89*, 371−377.
(75) (a) Cantley, L. C.; Aisen, P. *J. Biol. Chem.* **1979**, *254*, 1781−1784. (b) Heinz, A.; Rubinson, K. A.; Grantham, J. J. *J. Lab. Clin. Med.* **1982**, *100*, 593−611.

DOI: 10.1021/ic5028948
Inorg. Chem. 2015, 54, 6707−6718